HEIGHT–VELOCITY DIAGRAM ANALYSIS OF A VARIABLE SPEED ROTOR HELICOPTER

Xufei YAN, Cheng CHI, Renliang CHEN

crlae@nuaa.edu.cn

National Key Laboratory of Science and Technology on Rotorcraft Aeromechanics

Nanjing University of Aeronautics and Astronautics, China

Abstract

This paper applies optimal control method to study the effects of variable speed rotor (VSR) on the helicopter Height–Velocity (H-V) diagram in one engine inoperative (OEI) situation. Taken UH-60A as a sample helicopter, a flight dynamics model and the optimal control method applied are validated against the flight test data. The low-speed H-V diagram in OEI and the landing procedures at three key points (High hover, Knee and Low hover points) of the H-V diagram in OEI are investigated under different rotor operating speeds. Results indicate that the reduction of rotor operating rotation speed will cause the area of H-V diagram in OEI gradually shrink at first, and then expand rapidly. The rotor operating speed corresponding to the minimum area of H-V diagram in OEI is a little higher than that corresponding to the minimum required power. A reasonable rotor operating rotation speed not only effectively reduces the helicopter required power, but also improves the landing performance in OEI.

1. INTRODUCTION

The variable speed rotor (VSR) system is developed to reduce the rotor required power and improve helicopter flight performance. Therefore, VSR is now applied into some of the cutting edge rotorcrafts, e.g., the X2 coaxial helicopter using the Advancing Blade Concept (ABC), the V-22 tilt-rotor aircraft and the A160T long range unmanned aircraft [1]. Currently, various researches [2-4] have been conducted to improve the performance of VSR, including the studies of required power, fuel consumption, range, endurance, vibration level, etc. However, the effects of VSR on the helicopter landing performance in one engine inoperative (OEI) situation haven't been considered yet. The variation of rotor speed alters the kinetic energy stored in the rotor, which is crucial to the landing procedure in OEI. From a holistic standpoint, it is imperative to consider the landing performance in OEI when designing a VSR helicopter.

The helicopter landing performance after one engine failure can be intuitively reflected by the low-speed Height–Velocity (H-V) diagram in OEI [5-6], which is often described by a series of combinations of rotorcraft flight altitude and speed at the point of engine failure. The H-V diagram shows pilot the unsafe region to stay away during normal operation, therefore maximizing survival in the event of an unexpected engine failure. In general, flight tests are the ultimate methods to obtain the H-V diagram in OEI. However, they are very risky, time-consuming and expensive. In order to reduce the risks and costs, optimal control method has been proposed to predict the H-V diagram in OEI and the optimal safe landing procedure to provide a reference for flight tests [5-6]. Optimal control method is widely used in the research of helicopter safe flight after engine failure to provide pilot with unsafe region as well as the flight guidance and training [7-10].

Therefore, the effects of VSR on the helicopter low-speed H-V diagram in OEI are studied by applying the optimal control method. A UH-60A Black Hawk helicopter is taken as the sample helicopter. An augmented six-degree-of-freedom flight dynamics model is developed for landing trajectory optimization in OEI. The influence of rotor rotation speed on helicopter required power and collective control is studied to help determine the lowest feasible rotor operating rotation speed in stable level flight. Finally, the low-speed H-V diagram in OEI and the corresponding landing procedures at three key points (High hover, Knee and Low hover points) of the H-V diagram in OEI

Presented at 44th European Rotorcraft Forum, Delft, The Netherlands, 19-20 September, 2018

are investigated and analysed under different rotor operating rotation speeds.

2. FLIGHT DYNAMICS MODEL

First, a six-degree-freedom rigid body flight dynamics model of a UH-60A helicopter is given (see Ref. [11] for detailed modeling and verification process). It is formulated with both the rigid body dynamics and high-order dynamics of the main rotor. A brief introduction of the model is given below:

1. The aerodynamic forces and moments acting on the main rotor are calculated using blade element theory. Pitt-Peters' three-state dynamic inflow model [12] is used to predict the dynamics inflow of main rotor. The airfoil lift and drag coefficients of blade elements are obtained with an interpolation method based on the wind tunnel test data. The Leishman-Beddoes unsteady and dynamic stall model [13] is used to account for unsteady phenomena, flow separation, dynamic stall and transonic compressibility effects.
2. The main rotor blades are assumed to be rigid bodies, and the rigid flapping motions of each rotor blade are derived from the aerodynamic and inertial moment equilibrium at the hinge.
3. The fuselage, horizontal stabilizer and vertical fin are treated as rigid bodies. The aerodynamic force and moment coefficients are obtained with an interpolation method based on wind-tunnel test data.
4. The blade element theory is used to calculate the aerodynamic forces and moments generated by tail rotor as well, while the dynamic inflow of tail rotor is simulated by a one-state dynamic inflow model.

Finally, the state-space form of the model can be expressed as

$$\begin{cases} \dot{\boldsymbol{y}}_{\mathrm{b}} = f\left(\boldsymbol{y}_{\mathrm{b}}, \boldsymbol{u}_{\mathrm{b}}, t\right) \\ \dot{\boldsymbol{y}}_{\mathrm{b}} = [\boldsymbol{y}_{\mathrm{F}}, \boldsymbol{y}_{\mathrm{R}}, \boldsymbol{y}_{\mathrm{I}}]^{\mathrm{T}} \\ \boldsymbol{u}_{\mathrm{b}} = [\delta_{\mathrm{col}}, \delta_{\mathrm{lat}}, \delta_{\mathrm{lon}}, \delta_{\mathrm{p}}]^{\mathrm{T}} \end{cases} \tag{1}$$

where $\boldsymbol{y}_{\mathrm{F}}$ is the fuselage state vector, $\boldsymbol{y}_{\mathrm{R}}$ is the main rotor state vector, $\boldsymbol{y}_{\mathrm{I}}$ is the inflow state vector; δ_{col} is the collective stick input, δ_{lat} is the lateral stick input, δ_{lon} is the longitudinal stick input, and δ_{p} is the pedal input, t is the time.

When OEI occurs, the available power decreases from the all engine operating (AEO) power rating to the OEI power rating, the differential equations of main rotor operating speed Ω and available shaft power P_{A} can be described as [10]

$$\begin{aligned} \dot{\Omega} &= \frac{1}{\left(I_{\mathrm{R}} + k^2 I_{\mathrm{tR}}\right)\Omega}\left[P_{\mathrm{A}} - \frac{1}{\eta}\left(P_{\mathrm{mr}} - P_{\mathrm{tr}}\right)\right] \\ \dot{P}_{\mathrm{A}} &= \frac{1}{t_p}\left(P_{\mathrm{OEI}} - P_{\mathrm{A}}\right) \end{aligned} \tag{2}$$

where P_{mr}, P_{tr} are the power required by main and tail rotors, η is the helicopter power efficient factor, I_{R}, I_{tR} are the polar moments of inertia of main and tail rotors, k is the ratio of tail rotor speed to main rotor speed, t_p is the turboshaft engine time constant, and P_{OEI} is the maximum available power of the remaining engine.

In order to account for the limits on the control rates of the control vector $\boldsymbol{u}_{\mathrm{b}}$, and to avoid jump discontinuities arising in the time history of controls in the trajectory optimization [9-10], time derivatives of $\boldsymbol{u}_{\mathrm{b}}$ are applied as the control variables, denoted by $\boldsymbol{u}$. In the meantime, the $\boldsymbol{u}_{\mathrm{b}}$ is regarded as the state variables. The corresponding differential equations can be expressed as

$$\begin{cases} \dot{\delta}_{\mathrm{col}} = u_{\mathrm{col}} \\ \dot{\delta}_{\mathrm{lon}} = u_{\mathrm{lon}} \\ \dot{\delta}_{\mathrm{lat}} = u_{\mathrm{lat}} \\ \dot{\delta}_{\mathrm{p}} = u_{\mathrm{p}} \end{cases} \tag{3}$$

Equations (1) – (3) form an augmented flight dynamics model, which is suitable for helicopter landing trajectory optimization in OEI. The state-space form of the model can be expressed as

$$\dot{\boldsymbol{y}} = f\left(\boldsymbol{y}, \boldsymbol{u}, t\right) \tag{4}$$

where $\boldsymbol{y}$ and $\boldsymbol{u}$ are state vector and control vector, respectively:

$$\begin{cases} \boldsymbol{y} = \left[\boldsymbol{y}_{\mathrm{F}}, \boldsymbol{y}_{\mathrm{R}}, \boldsymbol{y}_{\mathrm{I}}, \Omega, P_{\mathrm{A}}, \boldsymbol{u}_{\mathrm{b}}\right]^{\mathrm{T}} \\ \boldsymbol{u} = [u_{\mathrm{col}}, u_{\mathrm{lat}}, u_{\mathrm{lon}}, u_{\mathrm{p}}]^{\mathrm{T}} \end{cases} \tag{5}$$

3. OPTIMAL CONTROL METHOD

The key of predicting H-V diagram in OEI is the calculation of safe landing procedure after one engine failure. The helicopter is considered in the unsafe region of H-V diagram in OEI if the safe landing procedure after one engine failure cannot be obtained at current flight speed and altitude. Therefore, based on the augmented flight dynamics model, the low speed H-V diagram and the corresponding safe landing procedure in OEI are determined by applying the optimal control method with the assumptions of average piloting skills and steady-state conditions before one engine failure.

Presented at 44th European Rotorcraft Forum, Delft, The Netherlands, 19-20 September, 2018

3.1. Nonlinear Optimal Control Problem

The safe landing procedure can be formulated as a nonlinear optimal control problem (NOCP), which can be expressed as following,

Optimal variables: differential state variables $\boldsymbol{y}$, control variables $\boldsymbol{u}$ of the flight dynamics model and the free final time t_f.

Cost function: in this paper, the cost function is formulated into the following general expression.

$$\begin{aligned}\min J &= w_\mathrm{t} t_\mathrm{f} + w_u \cdot u_d(t_\mathrm{f}) + w_w \cdot w_d(t_\mathrm{f}) \\ &+ \frac{1}{t_\mathrm{f} - t_0}\int_{t_0}^{t_\mathrm{f}} L\left[\boldsymbol{u}(t),\varphi(t),\psi(t)\right]\mathrm{d}t\end{aligned} \tag{6}$$

where

$$\begin{aligned}L\left[\boldsymbol{u}(t),\varphi(t),\psi(t)\right] &= w_1 \cdot u_\mathrm{c}^2 \big/ u_\mathrm{c,max}^2 + w_2 \cdot u_\mathrm{lat}^2 \big/ u_\mathrm{lat,max}^2 \\ &+ w_3 \cdot u_\mathrm{lon}^2 \big/ u_\mathrm{lon,max}^2 + w_4 \cdot u_\mathrm{p}^2 \big/ u_\mathrm{p,max}^2 \\ &+ w_5 \cdot \varphi^2 \big/ \varphi_\mathrm{max}^2 + w_6 \cdot \psi^2 \big/ \psi_\mathrm{max}^2\end{aligned} \tag{7}$$

u_d and w_d are the forward flight speed and decline rate; t_0 is the initial time; $u_\mathrm{c,max}$, $u_\mathrm{lat,max}$, $u_\mathrm{lon,max}$, $u_\mathrm{p,max}$ are the maximum value of four control rates; φ_max and ψ_max are the maximum allowable roll and yaw angle, respectively; w_t, w_u, w_w, w_1, w_2, w_3, w_4, w_5, w_6 are weight factors. The greater the weight factor, the more important the corresponding term is. In the landing procedure after one engine failure, the pilot mainly focuses on the control sticks while maintaining the attitude angles. Therefore, the weight factors w_1, w_2, w_3, w_4 (corresponding to control variables $\boldsymbol{u}$) are greater. The weight coefficient used in this paper is obtained by a large number of simulation tests, and the specific values will be given in the validation section.

The first 3 terms of the Eq. 6 represent the terminal state performance, and the last term represents the state and control performance of the whole landing procedure. The NOCP can be successfully solved if the time history of the control vector $\boldsymbol{u}(t)$ that minimizes the cost function is found under the following constraints.

Constraints: the constraints consist of differential equation, initial boundary conditions, path constraints and terminal constraints.

The differential equation is the state-space form of the augmented flight dynamics model (Eq.4).

The initial boundary conditions are determined in the moment of initial pilot control actuation after engine failure. Normally, pilot delay time t_d should be considered and applied for NOCP after engine failure recognition before pilot operation [14], thus the initial time t_0 of the NOCP equals to pilot delay time t_d here. During the delay period, the pilot is assumed to hold the controls fixed. To account for the pilot delay and obtain the corresponding values of the initial optimal variables ($\boldsymbol{y}_\mathrm{delay}$, $\boldsymbol{u}_\mathrm{delay}$) at time t_0, the differential equations is integrated for t_d second at the moment of one engine failure with controls fixed to the initial trim values, using the backward differentiation formulas. Hence the initial boundary conditions at t_0 can be described as

$$\boldsymbol{y}(t_0)=\boldsymbol{y}_\mathrm{delay},\quad \boldsymbol{u}(t_0)=\boldsymbol{u}_\mathrm{delay} \tag{8}$$

The path constraints of states are properly selected according to the specific safety-related requirements and helicopter performance limits, and the constraints of the control rates $\boldsymbol{u}$ are selected according to the maximum physical rate limits of the servo booster,

$$\begin{cases}\boldsymbol{y}_\mathrm{min} \le \boldsymbol{y}(t) \le \boldsymbol{y}_\mathrm{max} \\ \boldsymbol{u}_\mathrm{min} \le \boldsymbol{u}(t) \le \boldsymbol{u}_\mathrm{max}\end{cases} \tag{9}$$

The terminal constraints at t_f are properly selected according to the specific requirements of FAR for rotorcraft safe landing in engine failure situations [14],

$$\boldsymbol{y}_\mathrm{f,min} \le \boldsymbol{y}(t_\mathrm{f}) \le \boldsymbol{y}_\mathrm{f,max} \tag{10}$$

The specific path constraints and terminal constraints will be given in the validation section.

3.2. Numerical Solution Techniques

To improve computational efficiency and rate of convergence in the numerical optimization, the optimal variables of the NOCP are normalized and scaled first,

$$\begin{cases}\left(\bar{u},\bar{v},\bar{w}\right) = \dfrac{1}{k_v \Omega_0 R}\left(u,v,w\right) \\ \left(\bar{p},\bar{q},\bar{r}\right) = \dfrac{k_x}{k_v \Omega_0}\left(p,q,r\right) \\ \left(\bar{x},\bar{y},\bar{h}\right) = \dfrac{1}{k_x R}\left(x,y,h\right) \\ \bar{\Omega} = \dfrac{\Omega}{\Omega_0},\quad \bar{P}_\mathrm{A} = \dfrac{k_x}{k_v \Omega_0^3\left(I_\mathrm{R} + k^2 I_\mathrm{tR}\right)} P_\mathrm{A} \\ \tau = \dfrac{k_v \Omega_0}{k_x} t,\quad \bar{\boldsymbol{u}} = \dfrac{k_x}{k_v \Omega_0}\boldsymbol{u}\end{cases} \tag{11}$$

where u, v, w are the velocity components of helicopter in body axes; p, q, r are the roll, pitch and yaw angular rates; x, y, h are the helicopter longitudinal, lateral and height positions; k_x, k_v are scaling factors; Ω_0 is the helicopter standard rotor operating rotation speed, R is the main rotor radius. In order to make the normalized-scaled optimal variables close to one in value, take k_x=10 and k_v=0.1.

The normalized-scaled augmented flight dynamics model can be described as

$$\frac{\mathrm{d}\bar{\boldsymbol{y}}}{\mathrm{d}\tau} = f\left(\bar{\boldsymbol{y}},\bar{\boldsymbol{u}},\tau\right) \tag{12}$$

Presented at 44th European Rotorcraft Forum, Delft, The Netherlands, 19-20 September, 2018

where

$$(13)\quad \begin{cases} \bar{\boldsymbol{y}} = \left[\bar{\boldsymbol{y}}_{\mathrm{F}}, \boldsymbol{y}_{\mathrm{R}}, \boldsymbol{y}_{\mathrm{I}}, \bar{\Omega}, \bar{P}_{\mathrm{A}}, \bar{\boldsymbol{u}}_{\mathrm{b}} \right]^{\mathrm{T}} \\ \bar{\boldsymbol{u}} = [\bar{u}_{\mathrm{col}}, \bar{u}_{\mathrm{lat}}, \bar{u}_{\mathrm{lon}}, \bar{u}_{\mathrm{p}}]^{\mathrm{T}} \end{cases}$$

The most effective method to solve the NOCP at present is to transcribe it into a discrete nonlinear programming problem (NLP), which can be then solved by applying the sequential quadratic programming (SQP) method [15]. In this study, direct multiple shooting algorithm is used to fulfill such a transcription. This collocation method is typically used in the optimal control problems with large degree of freedom and medium or high complexity [16-17]. Hence, it is suitable for the NOCP established in this study. The base theory is shown in Fig. 1.

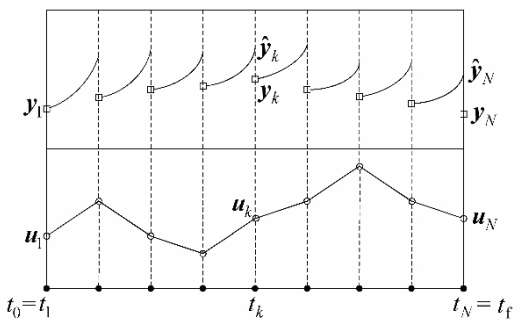

Fig. 1. Direct multiple shooting method

As shown in Fig. 1, the solution time interval [τ_0, τ_{f}] of the NOCP is divided into N-1 equal time segments:

$$(14)\quad \begin{cases} \tau_0 = \tau_1 < \tau_2 \cdots < \tau_k \cdots < \tau_N = \tau_{\mathrm{f}} \\ \tau_k = \tau_{k-1} + \Delta\tau \\ \Delta\tau = \left(\tau_{\mathrm{f}} - \tau_0\right) / \left(N-1\right) \end{cases}$$

In each time node, the discrete optimal variables are formed as follow:

$$(15)\quad \boldsymbol{Y} = \left[\left(\bar{\boldsymbol{y}}, \bar{\boldsymbol{u}}\right)_1, \left(\bar{\boldsymbol{y}}, \bar{\boldsymbol{u}}\right)_2, \ldots, \left(\bar{\boldsymbol{y}}, \bar{\boldsymbol{u}}\right)_k, \ldots, \left(\bar{\boldsymbol{y}}, \bar{\boldsymbol{u}}\right)_N, \tau_{\mathrm{f}} \right]$$

For the k^{th} segment, integrating the equation of state (Eq. 12) from τ_k to τ_{k+1} using the time stepping approach with piecewise linear interpolation of $\bar{\boldsymbol{u}}_k$ and $\bar{\boldsymbol{u}}_{k+1}$. Denote the result of this integration by $\hat{\bar{\boldsymbol{y}}}_{k+1}$, thus the shooting of segment k can be represented by as:

$$(16)\quad \bar{\boldsymbol{y}}_{k+1} - \hat{\bar{\boldsymbol{y}}}_{k+1} = \boldsymbol{0}, \quad k = 1, \cdots, N-1$$

where

$$(17)\quad \hat{\bar{\boldsymbol{y}}}_{k+1} = \bar{\boldsymbol{y}}_k + \int_{\tau_k}^{\tau_{k+1}} f(\bar{\boldsymbol{y}}, \bar{\boldsymbol{u}}, \tau) d\tau$$

The same treatment is implemented to the cost function:

$$(18)\quad \begin{aligned} \min \bar{J} = {} & w_{\mathrm{t}} \tau_N + w_u \cdot \bar{u}_d(\tau_N) + w_w \cdot \bar{w}_d(\tau_N) \\ & + \frac{1}{\tau_N - \tau_1} \sum_{k=1}^{N-1} \int_{\tau_k}^{\tau_{k+1}} L\left(\bar{\boldsymbol{u}}, \varphi, \psi\right) \mathrm{d}\tau \end{aligned}$$

Afterwards, the path constraints, initial boundary conditions and terminal constrains can be applied to each discrete node, initial node and terminal node, respectively.

$$(19)\quad \begin{cases} \bar{\boldsymbol{y}}_{\min} \le \bar{\boldsymbol{y}}_k \le \bar{\boldsymbol{y}}_{\max} \\ \bar{\boldsymbol{u}}_{\min} \le \bar{\boldsymbol{u}}_k \le \bar{\boldsymbol{u}}_{\max}, \quad k = 1, \cdots, N \end{cases}$$

$$(20)\quad \begin{cases} \bar{\boldsymbol{y}}_1 = \bar{\boldsymbol{y}}_{\mathrm{delay}}, \quad \bar{\boldsymbol{u}}_1 = \bar{\boldsymbol{u}}_{\mathrm{delay}} \\ \bar{\boldsymbol{y}}_{\mathrm{f}\min} \le \bar{\boldsymbol{y}}_N \le \bar{\boldsymbol{y}}_{\mathrm{f}\max} \end{cases}$$

The optimal solution of the NOCP is obtained by solving the NLP with SQP method. Finally, piecewise linear interpolation is used to construct an approximation to the continuous optimal control procedure $\boldsymbol{u}(t)$ of the NOCP, and the approximation of the continuous optimal states $\boldsymbol{y}(t)$ are obtained by integrating the differential equation (4) from t_0 to t_{f}.

3.3. Validation of Optimal Control Method

The flight test data of UH-60A helicopter landing procedure in OEI [18] is used to validate the flight dynamics model and the optimal control method. For conventional UH-60A helicopter with a constant speed rotor (CSR), the rotor operating rotation speed (Ω_0) is 27 rad/s, and the rotor rotation speed is strictly limited within 90% ~ 110%Ω_0 during whole landing procedure. The OEI initial conditions are steady-state with weight of 7103 kg, altitude of 13.7 m, forward speed of 5.1 m/s, track angle of 0°, and no sideslip, pilot delay t_{d} =1.7 s.

The specific terminal constraints are determined according to the requirements of FAR for rotorcraft safe landing in engine failure situation [14] as follows,

$$(21)\quad \begin{cases} -1^\circ/\mathrm{s} \le p(t_{\mathrm{f}}), q(t_{\mathrm{f}}), r(t_{\mathrm{f}}) \le 1^\circ/\mathrm{s} \\ -5^\circ \le \theta(t_{\mathrm{f}}) \le 10^\circ \\ -2^\circ \le \varphi(t_{\mathrm{f}}), \psi(t_{\mathrm{f}}) \le 2^\circ \\ 0 \le \dot{x}(t_{\mathrm{f}}) \le 12.2\,\mathrm{m/s} \\ -1 \le \dot{y}(t_{\mathrm{f}}) \le 1\,\mathrm{m/s} \\ -1.524 \le \dot{h}(t_{\mathrm{f}}) \le 0\,\mathrm{m/s} \\ 0 \le h(t_{\mathrm{f}}) \le 0\,\mathrm{m} \end{cases}$$

where φ, θ, ψ are the roll, pitch and yaw angles; $\dot{x}$ is the forward speed, $\dot{y}$ is the lateral speed, $\dot{h}$ is the rising speed.

Presented at 44th European Rotorcraft Forum, Delft, The Netherlands, 19-20 September, 2018

The specific path constraints are determined according to the flight mission, safety-related requirements and helicopter performance limits, and the constraints of the control rates are selected according to the control system characteristics [9] for Category-A helicopter safe flight after one engine failure.

$$
\begin{cases}
0 \le u(t) \le 40\,\mathrm{m/s} \\
-15 \le v(t) \le 15\,\mathrm{m/s} \\
-20 \le w(t) \le 20\,\mathrm{m/s} \\
-20 \le p(t), q(t), r(t) \le 20\,^\circ/\mathrm{s} \\
-20 \le \varphi(t), \theta(t), \psi(t) \le 20^\circ \\
0 \le h(t) \le 120\mathrm{m} \\
-20 \le y(t) \le 20\mathrm{m} \\
0 \le x(t) \le 200\mathrm{m} \\
0.9\Omega_0 \le \Omega(t) \le 1.1\Omega_0 \\
P_{\mathrm{OEI}} \le P_{\mathrm{A}}(t) \le P_{\mathrm{AEO}} \\
0 \le \delta_{\mathrm{c}}(t), \delta_{\mathrm{lat}}(t), \delta_{\mathrm{lon}}(t), \delta_{\mathrm{p}}(t) \le 100\% \\
-30 \le u_{\mathrm{c}}(t), u_{\mathrm{lat}}(t), u_{\mathrm{lon}}(t), u_{\mathrm{p}}(t) \le 30\,\%/\mathrm{s}
\end{cases} \tag{22}
$$

The weight factors of cost function are set as: w_t=0.01, w_u=0.03, w_w=0.03, w_1=w_2=w_3=w_4=0.15, w_5=w_6= 0.12.

Figure 2 shows the calculated optimal landing procedure in OEI as well as the flight test data. As can be seen, there is a good agreement between the prediction values and flight test data. The flight dynamics model and the optimal control method applied in this paper can be used to predict the safe landing procedure in OEI accurately.

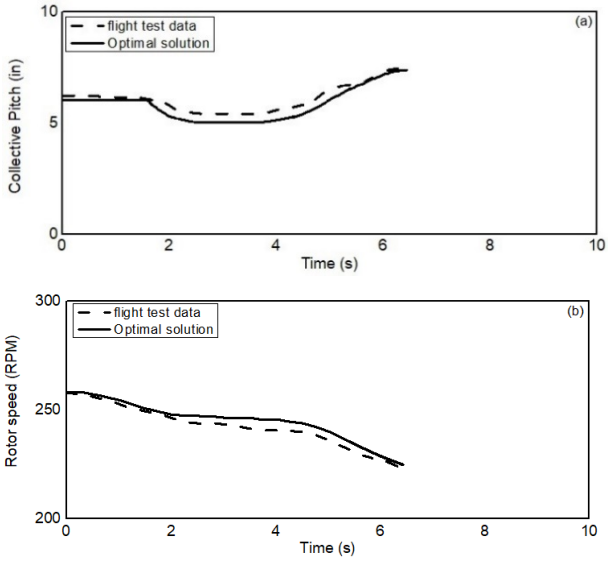

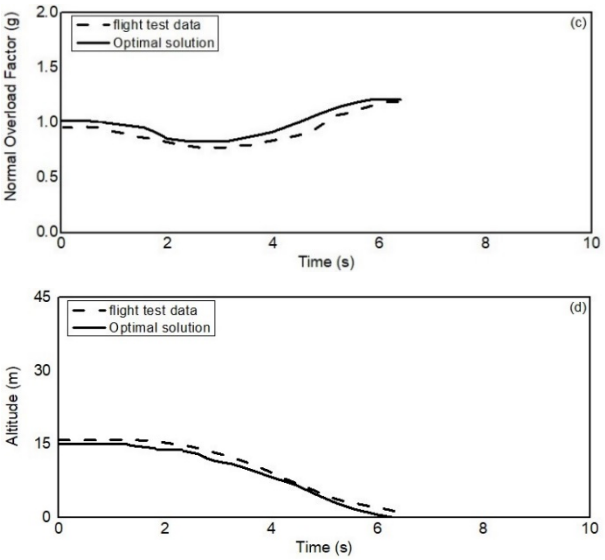

Fig. 2. Calculated optimal landing procedure in OEI vs. the flight test data: (a) collective pitch, (b) rotor speed, (c) normal overload factor, (d) altitude.

4. PREDICTION OF H-V DIAGRAM IN OEI

The accurate prediction of landing procedure in OEI in the last section indicates that the helicopter low-speed H-V diagram in OEI can be predicted by the augmented flight dynamics model proposed and optimal control method applied in this paper. The H-V diagram is the boundary curve of the unsafe region, which has three key points: high hover point, knee point and low hover point. The knee point divides the diagram into an upper boundary and a lower boundary. A helicopter is unable to make a safe landing after one engine failure when it flights between these two boundaries. Therefore, the H-V diagram in OEI directly reflects the helicopter landing performance after one engine failure.

As shown in Fig. 3, in order to search the boundary point of the H-V diagram in OEI under the given atmospheric environment and helicopter weight, the landing procedure in OEI at initial velocity V_0 (V_0=0 m/s) is firstly calculated with increasing height from h_0 (h_0=0 m) until the low hover point (V_0, h_1) and high hover point (V_0, h_2) can be determined. Then for any given height h between h_1 and h_2, a velocity sweep will be conduct until the successful landing procedure in OEI is found. By sweeping through the combination of height and velocity, all the boundary points corresponding to the successful and satisfactory landing procedures will be found. Figure 4 shows the calculation flow chart of H-V diagram in OEI.

Presented at 44th European Rotorcraft Forum, Delft, The Netherlands, 19-20 September, 2018

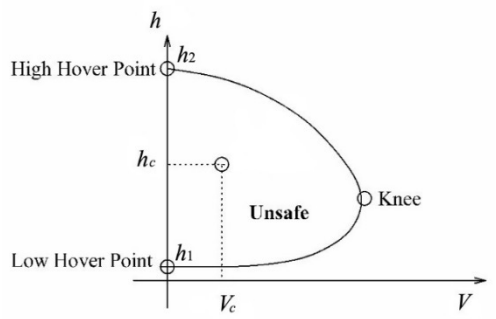

Fig. 3. Low-speed Height-Velocity diagram in OEI

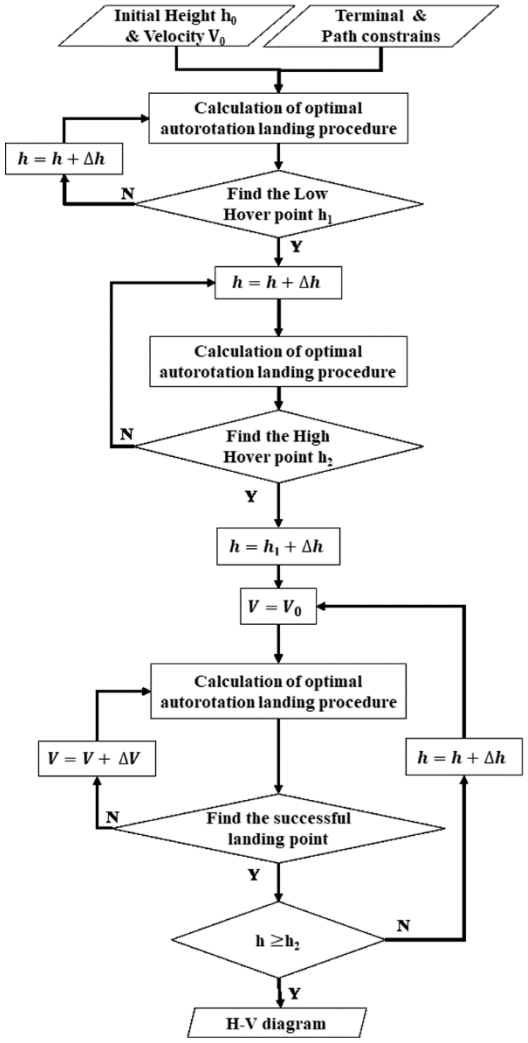

Fig. 4. Calculation Flow Chart of Height-Velocity Diagram in OEI

Figure 5 shows the low speed H-V diagram of UH-60A with CSR in OEI under different weights. The path constraints, terminal constraints and cost function are the same as those used in section 3.3. The results indicate that the unsafe region of H-V diagram in OEI will reduce as the helicopter gross weight decreases, and will finally vanish when the weight is below a certain value. To highlight the variation of H-V diagram in OEI, a helicopter gross weight of 9185 kg is chosen as the flight condition applied in the following discussions.

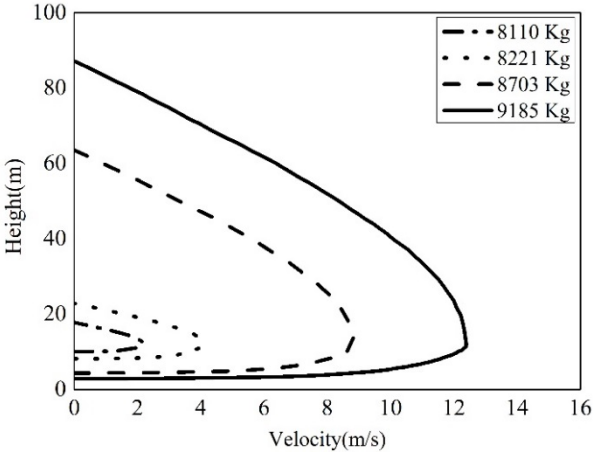

Fig. 5. H-V diagram in OEI with different gross weight of a CSR helicopter

5. EFFECTS OF VSR ON H-V DIAGRAM AND LANDING PROCEDURES IN OEI

For a helicopter with CSR, the kinetic energy of rotor that can be explored is limited by the extremely narrow rotor speed constraints (90% ~ 110%Ω_0), which is not conducive to the landing procedure in OEI. Comparing with the CSR helicopter, a VSR helicopter is capable of operating in a larger rotor speed range, which helps improve the landing performance in OEI.

5.1. Lowest rotor operating rotation speed in stable flight

As the rotor operating rotation speed reduces, the required power decreases, which is beneficial to improve flight performance. However, it will increase again when the rotor operating speed reduces below a certain value. This is because the expansion of the rotor reverse flow zone will lead to a greater rotor power loss. In addition, the helicopter will also encounter a trimming problem because of the control limitation. Therefore, it is necessary to obtain the lowest feasible rotor operating rotation speed in stable flight. This paper assumes that there is no additional limitation on the range of rotor rotation speed during VSR helicopter landing procedure in OEI, which means that the effects of rotor rotation speed on vibration level and aerodynamic noise are not considered here.

Figure 6a shows the helicopter required power and collective control stick at different rotor operating speeds in the low flight speed range. The results demonstrate that the required power decreases at first as the rotor operating speed reduces, and it starts to increase when the rotor operating speed reduces to 80%Ω_0. Moreover, the

Presented at 44th European Rotorcraft Forum, Delft, The Netherlands, 19-20 September, 2018

rotor collective stick position increases with the reduction of rotor operating rotation speed (Fig. 6b), and is approaching 100% limit at 76%Ω_0. Results in Fig. 6 indicate that 76%Ω_0 is the lowest feasible rotor operating rotation speed in stable flight for the sample helicopter in this paper.

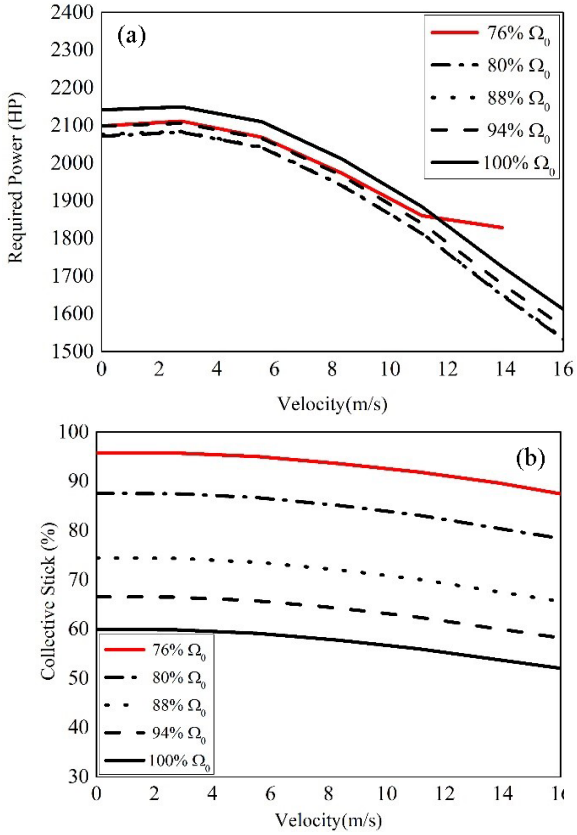

Fig. 6. Variation of helicopter required power and collective control with rotor speeds in low velocity range

5.2. Effects of VSR on H-V diagram in OEI

This section studies the effects of VSR on H-V diagram in OEI under different rotor operating rotation speeds. The path constraints, terminal constraints and cost function are the same as those used in section 3.3.

Figure. 7a shows that the area of H-V diagram in OEI shrinks gradually as the rotor operating rotation speed reduces from 100%Ω_0 to 84%Ω_0, while it expands rapidly when rotor operating speed reduces from 84%Ω_0 to 76%Ω_0. This is due to the gap between rotor required power and the maximum available power of the remaining single engine narrows as the rotor operating speed reduces, which is beneficial for helicopter landing in OEI. However, when the rotor speed reduces furthermore, the kinetic power stored in the rotor is not enough for a successful landing in OEI.

Figure 7b shows the H-V diagrams in OEI of UH60A VSR helicopter with 100%Ω_0, 84%Ω_0 (corresponding to the minimum area of H-V diagram in OEI), 80%Ω_0 (corresponding to the minimum required power in low speed, as shown in Fig. 6a) and 76%Ω_0. The H-V diagram in OEI for UH60A with 100%Ω_0 is also shown for comparison. As can be seen, the high hover point is getting lower as the rotor operating rotation speed reduces from 100%Ω_0 to 84%Ω_0. However, as the rotor speed reduces below 84%Ω_0, the height of high hover point increases while that of the low hover point decreases, together with the knee point moving outboard, which results in the expansion of H-V diagram in OEI. In addition, the rotor operating rotation speed corresponding to the minimum area of H-V diagram in OEI is a little higher than that corresponding to the minimum rotor required power. This is because although the helicopter required power is minimum at 80%Ω_0, the best landing performance still requires a little higher rotor operating rotation speed to store more kinetic energy, i.e. 84%Ω_0. The UH60A helicopter with a VSR in 80% ~ 100%Ω_0 has better landing performance in OEI situation than that with CSR.

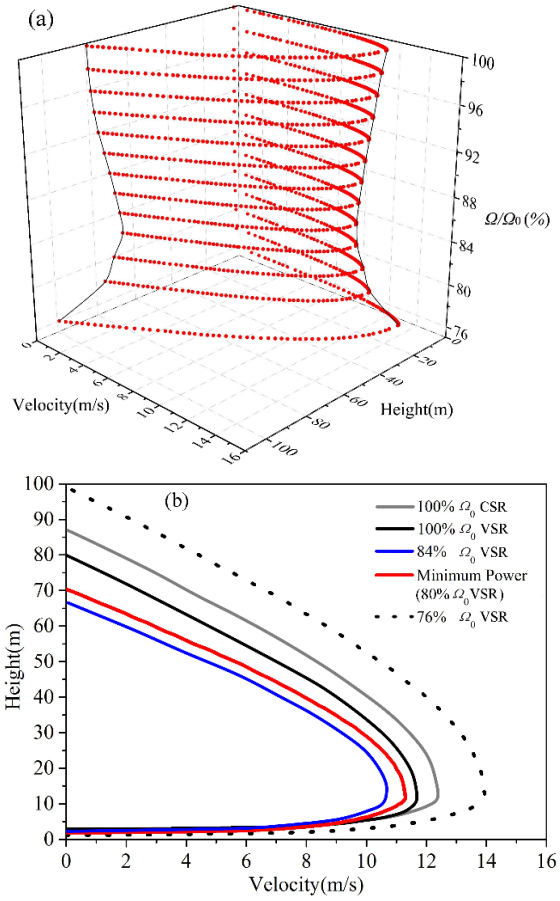

Fig. 7. Comparisons of H-V diagrams in OEI between different rotor operating speeds

5.3. Effects of VSR on landing procedures in OEI

Figure 8 shows the optimal time history of main rotor rotation speed and collective stick of the

Presented at 44th European Rotorcraft Forum, Delft, The Netherlands, 19-20 September, 2018

landing procedures at three key points (High hover, Knee and Low hover points) of the H-V diagram in OEI under different rotor operating rotation speeds (including CSR with 100%Ω_0).

As for the high hover point, the VSR is capable of operating in a larger rotor rotation speed range during the landing procedure in OEI, which allows the rotor to harvest more rotor kinetic energy for landing, while the rotor kinetic energy stored in CSR is strictly limited to be used.

For the knee point, the variation of main rotor rotation speeds and collective sticks are basically the same. This is because the forward flight speeds at knee point are all close to the maximum allowable touchdwon speed (i.e. 12.2 m/s), and the height is relatively low, hence the landing procedures in OEI are easier to be achived.

For the low point of the H-V diagram in OEI with 76%Ω_0, the collective control stick needs to hold at 100% of its displacement for almost 2 second. This means the loss of control margin which makes the helicopter vulnerable to any unexpected scenario.

Based on the above analysis in Fig. 8, the operating rotation speed of VSR between 80%Ω_0 and 84%Ω_0 is reasonable for the sample helicopter landing procedure in OEI. This is because the collective stick position still has a certain amount of control margin in the flight, hence the helicopter can make full use of the kinetic energy stored in the rotor. In addition, although the kinetic energy stored is less than that in the VSR with 100%Ω_0, the rotor required power is greatly deceased in the range of 80%Ω_0 ~ 84%Ω_0, hence the maximum available power of the remaining engine is able to make the landing procedure more smoothly.

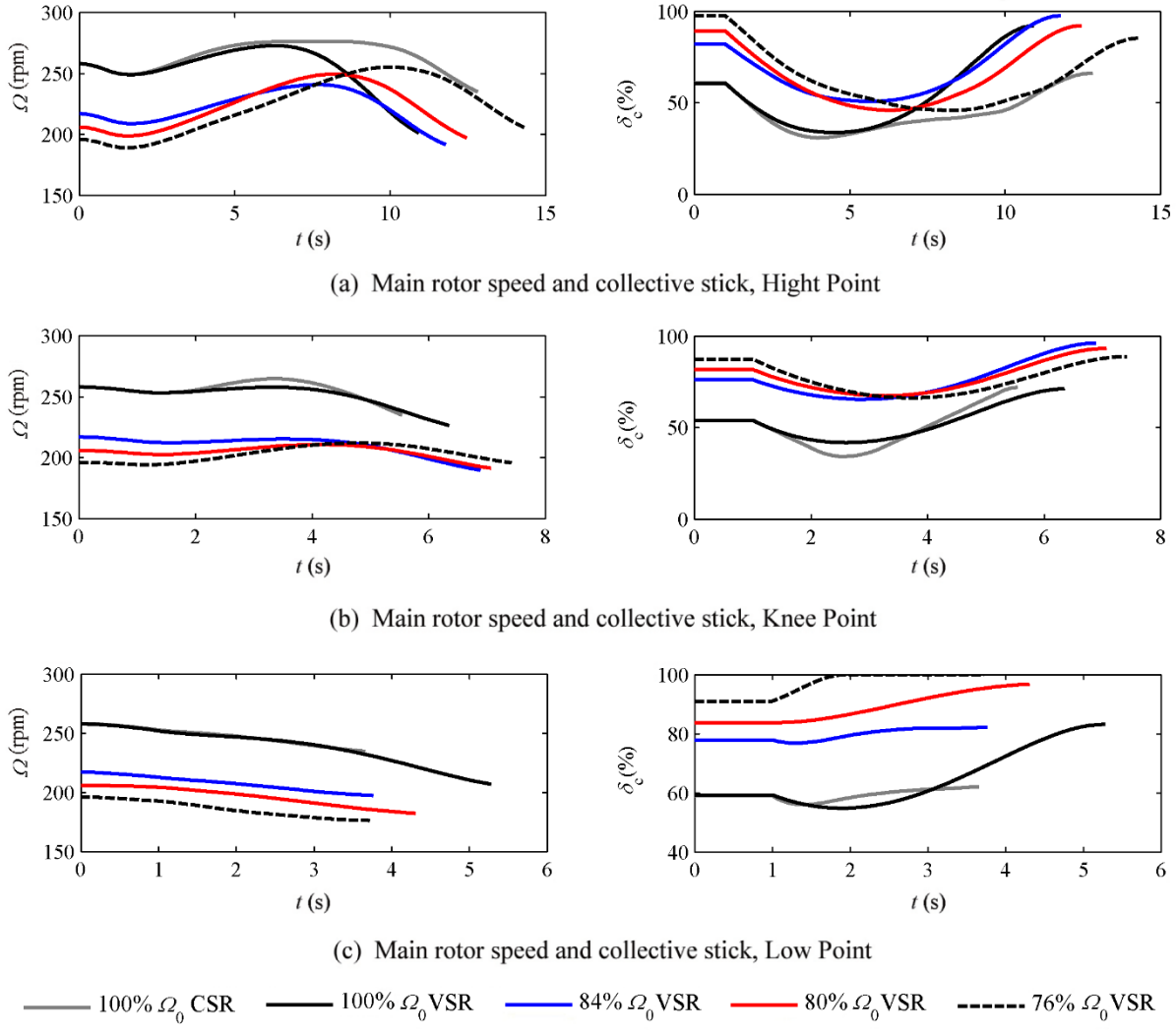

Fig. 8. Optimal main rotor speed and collective stick of the landing procedures in OEI at three key points

6. CONCLUSION

This work analyzes the VSR helicopter low-speed H-V diagram in OEI under different rotor operating rotation speeds by applying an augmented six-degree-of-freedom flight dynamics model and the optimal control method. A UH-60A helicopter with 9185 kg gross weight is taken as a sample

Presented at 44th European Rotorcraft Forum, Delft, The Netherlands, 19-20 September, 2018

helicopter. The investigation yields the following conclusions:

(1) As the rotor operating rotation speed reduces, the helicopter required power decreases effectively. However, the required power will increase again when the rotor operating speed reduces to 80% Ω_0. This is because the expansion of the rotor reverse flow zone will lead to a greater rotor power loss. In addition, the collective stick control input is approaching 100% limit at 76%Ω_0. Therefore, 76%Ω_0 is the lowest feasible rotor operating rotation speed in stable flight for the sample helicopter in this paper.

(2) The area of the H-V diagram in OEI shrinks gradually as the rotor operating rotation speed reduces from 100%Ω_0 to 84%Ω_0, while it expands rapidly when the rotor speed reduces from 84%Ω_0 to 76%Ω_0. The rotor operating rotation speed corresponding to the minimum area of H-V diagram in OEI is higher than that corresponding to the minimum required power, because although the helicopter required power is minimum at 80%Ω_0, the best landing performance still requires a little higher rotor operating rotation speed to store more kinetic energy, i.e. 84%Ω_0. The UH60A helicopter with a VSR in the range of 80% ~ 100%Ω_0 has better landing performance in OEI situation than a CSR.

(3) As for the high hover point, the VSR is capable of operating in a larger rotor speed range during the landing procedure, which allows the rotor to harvest more rotor kinetic energy for landing, while the rotor kinetic energy stored in CSR is strictly limited to be used. For the low point of the H-V diagram in OEI with 76%Ω_0, the loss of collective control margin will make the helicopter vulnerable to any unexpected scenario. In summary, the operating rotation speed of VSR between 80% ~ 84%Ω_0 is reasonable for the sample helicopter landing procedure in OEI. In that case, the collective stick still has a certain amount of control margin, hence the helicopter can make full use of the kinetic energy stored in the rotor. In addition, although the kinetic energy stored is less than that in the VSR with 100%Ω_0, the rotor required power is greatly decreased, which makes the maximum available power of the remaining engine easier to support the landing procedure in OEI.

REFERENCES

[1] Bowendavies G M, Chopra I. Aeromechanics of a Slowed Rotor[J]. Journal of the American Helicopter Society, 2015, 60(3): 032011-032011.

[2] DiOttavio J, Friedmann D. Operational benefits of an optimal, widely variable speed rotor[C]//Proceedings of AHS 66th Annual Forum, Phoenix. 2010, 1: 1865-1871.

[3] Bowen-Davies G, Chopra I. Aeromechanics of a variable-speed rotor[C]//American Helicopter Society 67th Annual Forum. 2011.

[4] BERRY B, CHOPRA I. Performance and Vibratory Load Measurements of a Slowed-Rotor at High Advance Ratios[C]//Proceedings of the 68th Annual Forum of the American Helicopter Society, Fort Worth, TX: AHS, 2012.

[5] Jhemi A A, Carlson E B, Zhao Y, et al. Optimization of rotorcraft flight following engine failure[J]. Journal of American Helicopter Society, 2004:117-126.

[6] Carlson E B, Xue S, Keane J, et al. H-1 upgrades height-velocity diagram development through flight test and trajectory optimization[C]//American Helicopter Society 62nd Annual Forum Proceedings, Phoenix, Arizona, May 2006, 62(2): 729-743.

[7] Aponso, B. L., and Bachelder, E. N. An autorotation flight director for helicopter training[C]//American Helicopter Society 59th Annual Forum Proceedings, Phoenix, Arizona, May 2003, 59(2): 1861-1872.

[8] Aponso B L, Lee D, Bachelder E N. Evaluation of a rotorcraft autorotation training display on a commercial flight training device[J]. Journal of the American Helicopter Society, 2007, 52(2): 123-133.

[9] Bottasso C. L., Maisano G., and Scorcelletti F. Trajectory optimization procedures for rotorcraft vehicles, their software implementation, and applicability to models of increasing complexity[J]. Journal of the American Helicopter Society, 2010, 55(3): 32010-32010.

[10] Meng, W., and Chen, R. Study of helicopter autorotation landing following engine failure based on a six-degree-of-freedom rigid-body dynamics model[J]. Chinese Journal of Aeronautics, 2013, 26(6):1380-88.

[11] Ji, H., Chen, R., and Li, P. Distributed Atmospheric Turbulence Model for Helicopter Flight Simulation and Handling-Quality Analysis[J]. Journal of Aircraft, 2016, 54(1):1-9.

[12] Frederick D. K., "Formulation and Validation of High-Order Mathematical Models of Helicopter Flight Dynamics," [D].University of Maryland College Park, 1991.

[13] Leishman J. G., and Beddoes T. S. A Semi-Empirical Model for Dynamic Stall[J]. Journal of the American Helicopter society, 1989, 34(3): 3-17.

[14] Kim, S. Certification of Transport Category Rotorcraft 29-2C[S]. Washington: Federal Aviation Administration, Department of Transportation; 2014. p. 57-146.

[15] Gill P E, Murray W, Saunders M A. SNOPT: An

Presented at 44th European Rotorcraft Forum, Delft, The Netherlands, 19-20 September, 2018

SQP algorithm for large-scale constrained optimization[J]. SIAM review, 2005, 47(1): 99-131.
[16] Kim, C. J., Sung, S., Park, S. H., Jung, S. N., Park, T. S. Numerical time-scale separation for rotorcraft nonlinear optimal control analyses[J]. Journal of Guidance, Control, and Dynamics, 2014, 37(2): 658-673.
[17] Bottasso, C. L., Maisano, G., Scorcelletti, F. Trajectory optimization procedures for rotorcraft vehicles including pilot models, with applications to ADS-33 MTES, CAT-A and engine off landings[C]//Proceedings of the 65th American Helicopter Society, Grapevine, TX, May 2009.
[18] Nagata, John I., et al. Government Competitive Test Utility Tactical Transport Aircraft System (UTTAS). Sikorsky YUH-60A Helicopter[R]. ARMY AVIATION ENGINEERING FLIGHT ACTIVITY EDWARDS AFB CA, 1976. No. USAAEFA-74-06-1.

Presented at 44th European Rotorcraft Forum, Delft, The Netherlands, 19-20 September, 2018